Aspartate Transcarbamylase (ATCase) of *Escherichia coli*: A New Crystalline R-State Bound to PALA, or to Product Analogues Citrate and Phosphate[†,‡]

Jingwei Huang and William N. Lipscomb*

Department of Chemistry and Chemical Biology, Harvard University, 12 Oxford Street, Cambridge, Massachusetts 02138

Received September 25, 2003; Revised Manuscript Received March 15, 2004

ABSTRACT: Structures of the R-state of *Escherichia coli* ATCase maintained with carbamyl phosphate and succinate, phosphonoacetamide and malonate, or *N*-phosphonacetyl-L-aspartate (PALA) have previously been made in the space group *P*321, in which the two independent r (regulatory) and two independent c (catalytic) chains are repeated by crystallographic symmetry to yield the holoenzyme c_6r_6, $((c_3)_2(r_2)_3)$. The exploration of a new crystalline R-state $P2_12_12_1$ was undertaken to examine the $c_3\cdots c_3$ expansion of 11 Å in the T-to-R transition, and to further test whether intermolecular contacts influence the binding of PALA. The results show that the expansion along the 3-fold axis is 10 Å, and that the binding modes of the six crystallographic independent PALA molecules are virtually identical to one another, and to modes described previously. As further test, the PALA, a bisubstrate analogue, was displaced by citrate and phosphate, where citrate is an analogue of product carbamylaspartate. The results support the conclusions about the binding of the three previously studied analogues, and further support, within about 0.5 Å, the structure proposed for the transition state [Gouaux, J. E., Krause, K. L., and Lipscomb, W. N. (1987) *Biochem. Biophys. Res. Commun. 142*, 893−897; Jin, L., Stec, B., Lipscomb, W. N., and Kantrowitz, E. R. (1999) *Proteins: Struct., Funct., Genet. 37*, 729−742].

The first step in many prokaryotes, including *Escherichia coli*, is the catalytic reaction of carbamyl phosphate and L-aspartate to yield carbamylaspartate and inorganic phosphate. The catalyst is the allosteric enzyme, aspartate transcarbamylase (ATCase,[1] EC 2.1.3.2). Homotropic regulation is controlled by the aspartate concentration, whereas heterotropic activation occurs by ATP (*1*) and heterotropic inhibition occurs by CTP or by CTP and UTP together (*2*). Thus, a balance is favored between pyrimidine triphosphates and purine triphosphates in biosynthesis of nucleic acid molecules.

All known ATCases, including also the multienzyme complexes of eukaryotic cells, are inhibited by *N*-phosphonacetyl-L-aspartate (PALA), which combines most of the structural features of the substrates carbamyl phosphate and aspartate (Figure 1), and binds (*3*) with a K_i of 27 nM. Following an early study (*4*) showing blocking of proliteration of mammalian cells in cultures, many studies have been made of the use of PALA by itself or along with other compounds in clinical trials of various cancers.

The dodecameric structure c_6r_6 of the *E. coli* ATCase was proved starting from the sequence of the regulatory chain (*5*) and independently from crystallographic symmetry determinations (*6*), thus correcting the earlier c_4r_4 model. The dodecamer consists of two catalytic trimers required by the crystallographic 3-fold axis, and three regulatory dimers related to one another also by this 3-fold axis. Structures of the T form (*7, 8*) and R form (*9, 10*) revealed the domain structures: the allosteric (Al) and zinc (Zn) domains of the r chain, and the carbamyl phosphate (CP) and aspartate (Asp) domains of the c chain. In the T-to-R transition the CP/Asp domains close around the substrates (or their analogues, or PALA), as the Al/Zn domains open. Most striking is the elongation of the enzyme along the 3-fold axis such that the $c_3\cdots c_3$ distance increases from 45.3 Å (*8*) to 56.1 Å (*10*), an elongation by 11 Å, accompanied by a rotation of one c_3 relative to the other by 12°, and a rotation of each of the three r_2's by about 15° around the three nonexact 2-fold axes of the dodecamer. These changes are even larger in studies of the low angle X-ray scattering in solution (*11, 12*).

In the present study, ATCase bound to six PALA molecules is described in a new crystalline form in the space group $P2_12_12_1$. The whole molecule is in the asymmetric unit such that the six PALA sites are independent of crystal symmetry. It is shown that binding of PALA to each of these six sites closely resembles that of the two independent PALA sites of the *P*321 crystalline form (*9, 10*). Moreover, the $c_3\cdots c_3$ distance is 55.4 Å along the molecular 3-fold axis, and thus the T-to-R elongation is 10 Å.

In addition, crystals were obtained of an analogue of products prepared upon displacement of PALA by citrate (an analogue of carbamylaspartate) and phosphate. The idea was to explore whether the product analogues were bound

[†] This work was supported by NIH Grant GM06920.

[‡] Structural data: coordinates have been deposited with Protein Data Bank as 1Q95 and 1R0B.

* To whom correspondence should be addressed. Department of Chemistry and Chemical Biology, Harvard University, 12 Oxford Street, Cambridge, MA 02138, USA. Phone: 617-495-4098. Fax: 617-495-3330. E-mail: lipscomb@chemistry.harvard.edu.

[1] Abbreviations: ATCase, aspartate transcarbamylase; PALA, *N*-phosphonacetyl-L-aspartate; ATP, adenosine 5′-triphosphate; CTP, cytidine 5′-triphosphate; UTP, uridine 5′-triphosphate; PDB, Brookhaven Protein Data Bank; 1D09, the R-state structure of aspartate transcarbamylase with PALA bound deposited in the Protein Data Bank determinated to 2.1 Å resolution; 6AT1, the T-state structure of aspartate transcarbamylase deposited in the Protein Data Bank determinated to 2.6 Å resolution; CP, carbamoyl phosphate; AL, allosteric; Cit, citrate; Pi, phosphate; NAC, near attack configuration; CHESS, Cornell High Energy Synchrotron Source.

10.1021/bi030213b CCC: $27.50
Published on Web 05/06/2004

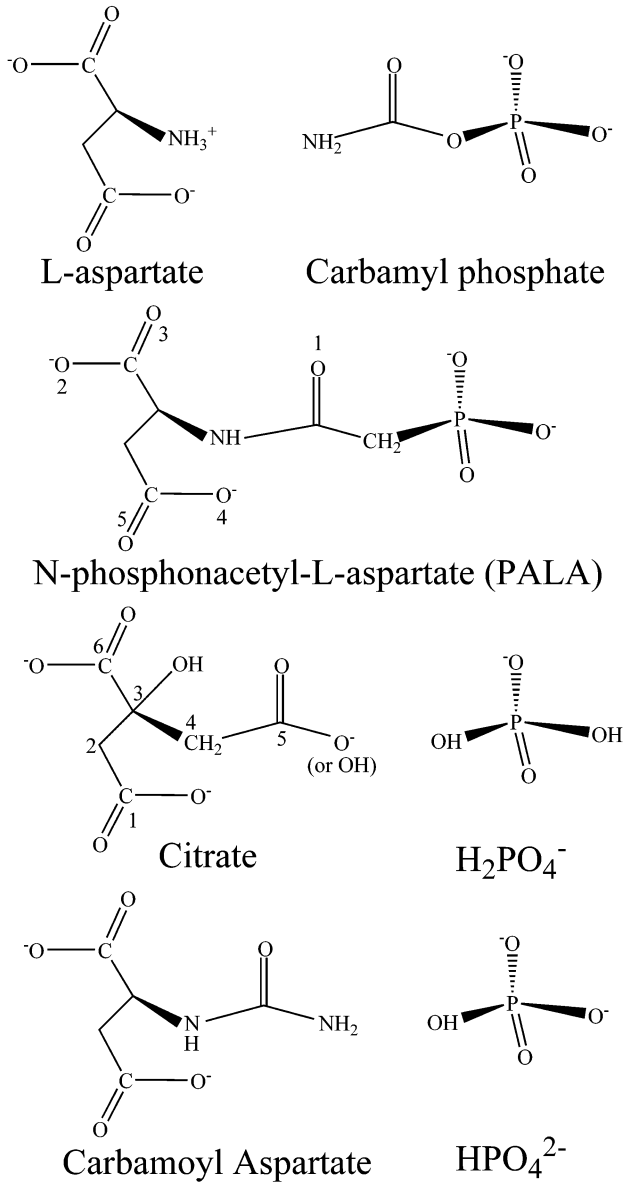

FIGURE 1: The chemical structures of the substrates, products, and their analogues.

close to the regions where substrate analogues are bound, or close to a product-leaving binding mode.

MATERIALS AND METHODS

Enzyme Purification and Crystallization. The holoenzyme of aspartate transcarbamylase was isolated by the methods of Nowlan and Kantrowitz (*13*) from the *E. coli* strain EK1104 containing the plasmid pEK54 (*14*). Crystals of PALA ligated enzyme were grown by hanging drop vapor diffusion: 2 μL of enzyme at 16 mg/mL in buffer (40 mM KH_2PO_4/0.2 mM EDTA/2 mM-mercaptoethanol, pH 7.0) were mixed with 7% (vol/vol) poly(ethylene glycol) methyl ether 2000 (PEG-mmes-2K)/0.16 M Li_2SO_4/3 mM NaN_3, and then equilibrated against 1 mL of 7% PEG-mmes-2K/0.16 M Li_2SO_4/3 mM NaN_3.

To displace PALA by citrate and phosphate for the second part of this study, the following procedure was started two weeks before collection of diffraction data. A single crystal of the PALA ligated enzyme was transferred along with mother liquid into a 10 μL microdialysis chamber, and then covered with a SPECTRUM (Spectra/Por) molecularporous dialysis membrane (MW cut off 12000−14000), and then completely immersed in 2 mL of buffer consisting of 10 mM Na_2HPO_4/10 mM sodium citrate/50 mM *N*-ethylmorpholine/ pH 5.8. The buffer was changed once every 24 h for 14 days. Preliminary X-ray diffraction results showed that citrate and phosphate had displaced PALA. At pH 5.8, the predominant species of citrate are citrate^{3-} (69.3%) and monoprotonated citrate (28.2%); the predominant species of phosphate is $H_2PO_4^-$ (96.2%). Porter et al. (*15*) observed that the K_i (apparent) for an inhibitor of ATCase shows a linear relationship with the reciprocal of the concentration of H^+. Thus, the enzyme−inhibitor complex will be less stable when pH increases. In addition, the inhibition of ATCase by citrate is weaker than that of other intermediates of the Krebs cycle, such as succinate and fumarate (*16*). Therefore, the pH of 5.8 will be more helpful than a higher pH to stabilize the enzyme−citrate−phosphate complex.

Table 1: Data Collection and Refinement Summary

description	wild-type ATCase with PALA	wild-type ATCase with citrate and phosphate
data collection location	CHESS	CHESS
space group	$P2_12_12_1$	$P2_12_12_1$
cell dimensions (Å)	$a = 125.5$	$a = 120.7$
	$b = 153.5$	$b = 155.4$
	$c = 185.7$	$c = 195.0$
	$\alpha = \beta = \lambda = 90°$	$\alpha = \beta = \lambda = 90°$
resolution limits (Å)	50−2.46	50−2.9
measured reflections	151,033	184,724
unique reflections	115,470	61,088
R_{merge}	0.077	0.077
$\langle I \rangle/\sigma$	8.7	14.9
completeness (%)	88.5	72.5
R value	0.23	0.24
R_{free} value	0.27	0.30
Luzzati coordinate error (Å)	0.38	0.47
bond lengths rms deviations (Å)	0.009	0.015
bond angles rms deviations (deg)	1.40	1.66
$C_3\cdots C_3$ distance (Å)	55.4	55.2
conformation	*R*-state	*R*-state

Data Collection and Structure Refinement. The X-ray data for ATCase with PALA, and for ATCase with citrate and phosphate were collected to 2.46 Å resolution for the former and 2.9 Å for the latter, both in the space group $P2_12_12_1$ (Table 1). The crystals were flash frozen to 100 K for data collection. For both structures, a catalytic trimer, which was constructed from PDB 1D09 with the PALA removed, was chosen as the search model. Then molecular replacement was performed by using AMORE (*17*). The initial structure model was built from the molecular replacement solution by adding the regulatory chains. Following rigid-body refinement of the holoenzyme, PALA, or citrate and phosphate were built into the simulated annealing omit map. The PALA model was taken from PDB 1D09, and citrate and phosphate models were from HIC-UP (*18*). Refinement of both structures was made using the CNS_SOLVE package (*19*), and visualized and modified against $2F_o - F_c$ maps and $F_o - F_c$ maps using the program O (*20*). Finally, the stereochemical properties of intermediate and final structures were examined by PROCHECK (*21*). Protein−protein interface interactions were calculated by Protein−Protein Interaction Server (*22*), and checked with O and Luzzati plots (*23*). Figures were

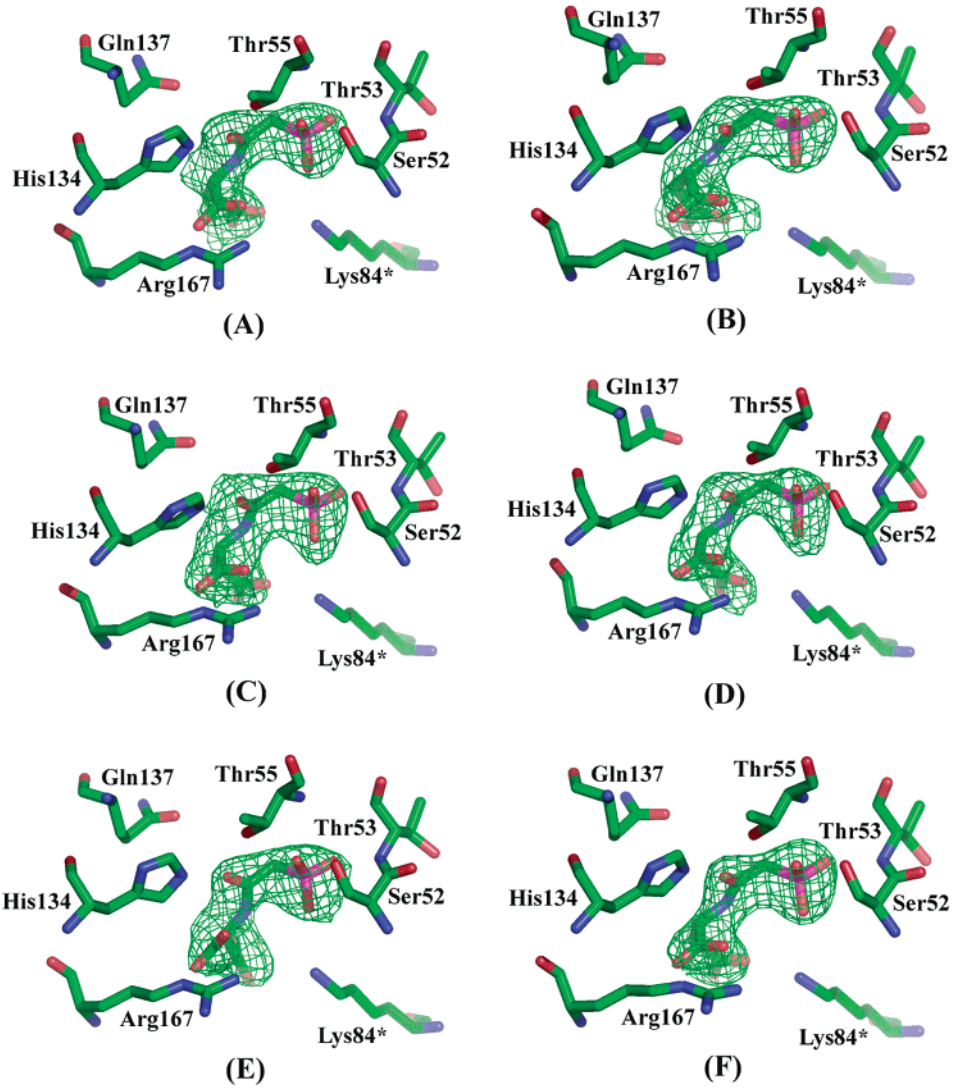

FIGURE 2: The ($F_o - F_c$) omit electron density (5σ) around PALA of the six active sites (A−F); Lys84* is from the adjacent catalytic chain. The literature contains many doubts about the one previously available R-state PALA−ATCase structure, which has two crystallographically independent PALA sites. The present study adds six independent sites, which confirm the PALA−ATCase binding mode. This mode is close to the binding modes of substrate analogues.

prepared using PyMOL (*24*), MOLSCRIPT (*25*), and BOBSCRIPT (*26*).

RESULTS

The Enzyme Structure in the PALA Complex. In the $P2_12_12_1$ space group, there are no crystallographic constraints other than the crystal packing. Nevertheless, the monomers within the c_3 trimers are related by a rotation of 120 ± 0.4°, and the trimers can be superimposed with a standard deviation of 2.5°. The relative rotation of one trimer (fixed) to the other is 15°, and the distance between the two trimers is increased by 10 Å over the distance in the T state (*P*321 form, PDB code 6AT1). Whereas the 3-fold molecular axis is well retained, the three 2-fold axes of the approximate D_3 symmetry are less exact. The comparison of regulatory dimers shows high rms deviations of 1.5−3.1 Å. In the catalytic chains the X-planar angles (*10*) defining the opening between the Asp and CP domains are 129°, 129°, 130°, 131°, 129°, and 129° for the six sites involving binding of PALA, about 1.2° to 3.6° larger than those in the 2.1 Å *P*321 PALA ligated structure (PDB code 1D09).

The consensus binding mode of PALA in the $P2_12_12_1$ structure is very much like that reported previously for the *P*321 structure. Interactions occur with Ser52, Thr53, Arg54, Thr55, Arg105, His134, Gln137, Arg167, Arg229, Gln231, and Ser80*, and Lys84* from an adjacent catalytic chain as designated by the asterisks. Only Leu267 was not found here to show a backbone carbonyl group interacting with the NH of PALA. The interaction of the amide NH of Glu137 with the backbone O of PALA showed weak interactions in the 3.5−4.0 range in the $P2_12_12_1$ structure but not in the *P*321 structure. However, Glu137 does show interactions to substrate carbamyl phosphate (*27*), substrate analogue phosphonoacetamide (*28*), and product analogue citrate (see below). This interaction of Glu137 was not seen in the 2.1 Å structure of the *P*321 complex with PALA.

Among the six sites (Figure 2) of the present study the side chains of Arg229 and Lys84* did not interact with O5 of PALA at site E, but the main chain carbonyl oxygen of Pro266 was found at this position. However, the many other interactions at site E were very similar to those at the other sites A, B, C, D, and F.

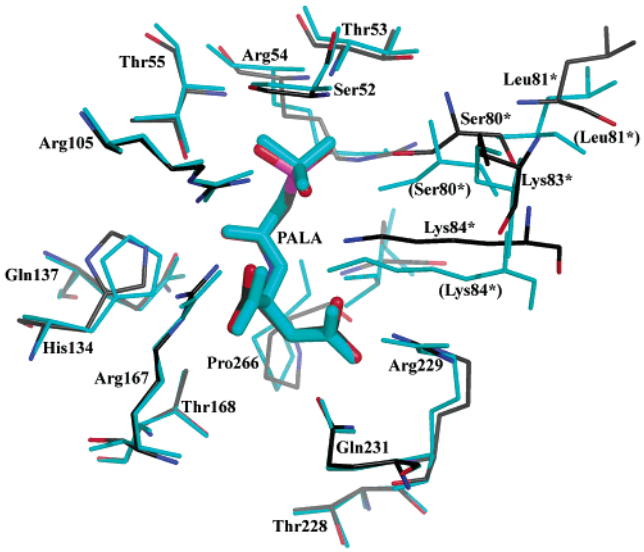

FIGURE 3: The superposition of the enzyme−PALA complex in $P2_12_12_1$ (black-blue-red, new) and in $P321$ (cyan, 1D09).

Other interactions are as follows. New polar interactions between Arg229 and Lys84* from the adjacent catalytic chain are found in the new structure. Compared to the R-state PALA−aspartate transcarbamylase complex at 2.1 Å resolution (Figure 3), it is clear that the flexible 80's loop moves to a new position in the new structure. This movement places the side chain of Lys84* close to the side chain of Arg229: distances are between 3.6 and 3.9 Å for the sites A−F. Although the 80's loops are around the active sites, the new positions of the 80's loops do not change the PALA binding mode. This movement of the 80's loops may be caused by the crystal packing.

The asymmetry among the catalytic and regulatory chains can also be reflected from the different interactions between catalytic and regulatory chains. The interactions of Asn13c−Lys137r, Thr87c−Glu119r, Gln108c−Asn113r, Glu109c−Lys143r, $^{\pm}$Gly110c−Tyr140r, Arg113c−Lys139r, Glu117c−Lys139r, Ser131c−Lys143r, Asn132−Cys141r, Asp200c−Arg128r, Asp200c−Arg130r are found only at some of the six catalytic (c) and the six regulatory (r) chains. Asn13c−Lys137r, Thr87c−Glu119r, Glu109c−Lys143r are new interactions, but the interactions of Gln108c−$^{\pm}$Cys114r, Glu109c−Asn111r, Arg113c−Glu142r, Asn132c−$^{\pm}$Tyr140r, Gln133c−Glu142r, Glu196c−Arg130r, Tyr197c−Lys143r, Asp200c−Glu144r, Glu204c−Arg128r in previous PALA ligated aspartate transcarbamylase are missing in the new structure. The symbol $\pm$ indicates a backbone interaction.

The ATCase Complex with Citrate and Phosphate. In the asymmetric unit of the $P2_12_12_1$ unit cell, there is one c_6r_6 molecule. Noncrystallographic symmetry among the six catalytic chains of the two c_3 trimers has standard deviations of 0.26−0.35 Å, and the approximate 3-fold axis has a rotation angle of 120° $\pm$ 0.4°. The relative rotation of one trimer relative to the other is 13°, and the R-state crystal shows an expansion of the $c_3\cdots c_3$ distance of 10 Å relative to the T-state along the molecular 3-fold axis. The six regulatory chains in the three r_2 units show rms deviations of 1.1−3.1 Å, and unequal rotations about the approximate

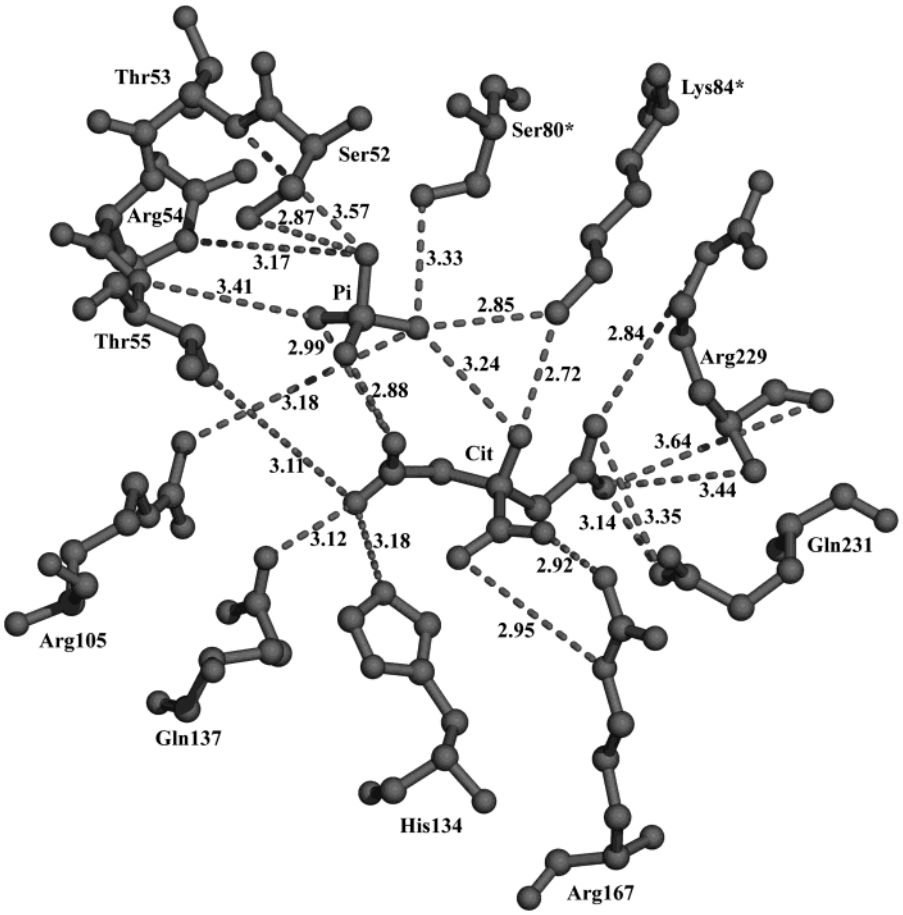

FIGURE 4: Binding of phosphate and citrate at the active site.

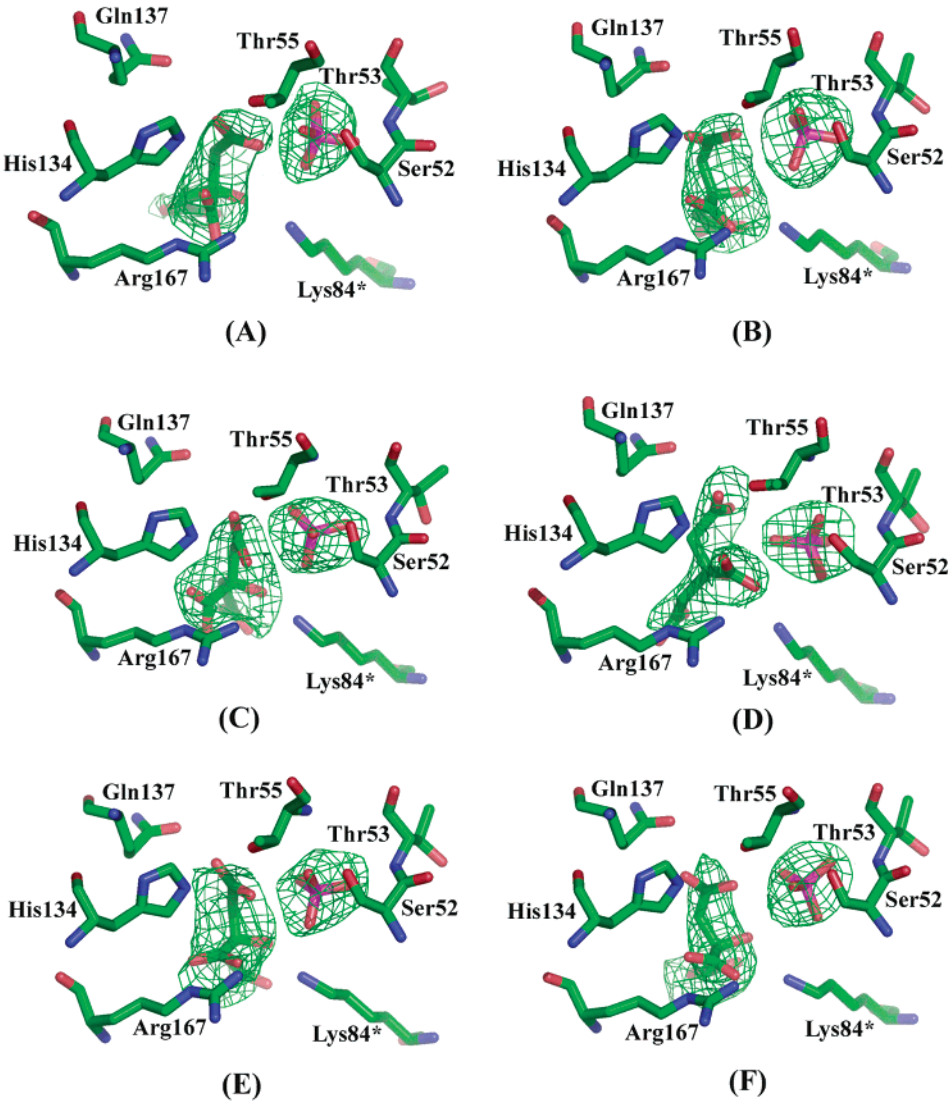

FIGURE 5: The ($F_o - F_c$) omit electron density (5σ) around the phosphate and citrate of the six active sites (A−F); Lys84* is from the adjacent catalytic chain.

2-fold axes of 20°, 17°, and 10°, although the average of 16° is consistent with previous studies of the T-to-R transition.

The phosphate interacts with main chain NH units of Thr53, Arg54, and Thr55, and with side chains of Ser52, Arg54, Thr55, Arg105, Ser80*, and Lys84*. (The asterisk indicates an adjacent catalytic chain of the c_3 trimer.) These and other interactions with citrate are summarized in Figure 4, including the 1-position carboxylate oxygen with Arg229 and Gln231, the 5-position carboxylate with Thr55, Gln137, His134 and phosphate, the 6-position carboxylate with Arg167 and Lys84* (adjacent chain), and the citrate OH with Lys84* and to an oxygen of phosphate. The distance between the carbon of the 5-carboxylate and the nearest phosphate oxygen averages to 3.3 Å: the six individual values are 2.9, 2.9, 3.1, 3.4, 3.6, and 4.0 Å. The six sites are shown at the contour level of 5σ in the $F_o - F_c$ electron density in Figure 5.

DISCUSSION

The $c_3 \cdots c_3$ increase of 10 Å in the T-to-R transition found here using the $P2_12_12_1$ R-state is not significantly different from the 11 Å increase when the *P*321 R-state is compared with the T state. A modeling study of the small-angle X-ray scattering experiments suggest in solution a further increment over 11 Å for the $c_3 \cdots c_3$ distance of 2.8 Å (total 13.8 Å) when PALA is bound, and of 4.4 Å (total 15.4 Å) when PALA + MgATP is bound to maintain a super R-state (*11*, *12*). Further attempts to obtain yet another R-state crystalline form are desirable to probe the structures of these elongated R-states.

The binding modes of PALA at the six crystallographic independent sites of the present study in space group $P2_12_12_1$ are very similar to the two independent modes in the earlier studies (*9*, *10*). These modes are also very similar to those in crystallographic studies of carbamyl phosphate (a substrate) plus succinate (an analogue of aspartate) (*27*) and of phosphonoacetamide (an analogue of carbamyl phosphate) plus malonate (an analogue of aspartate) (*28*).

PALA is bound strongly, with a K_i of 27 nM. However, PALA is a bisubstrate analogue, and the K_i is not far from the product of similar constants for the two substrates (*3*). Of course, PALA is not a perfect analogue for carbamyl phosphate and aspartate, because its carbamyl carbon is not

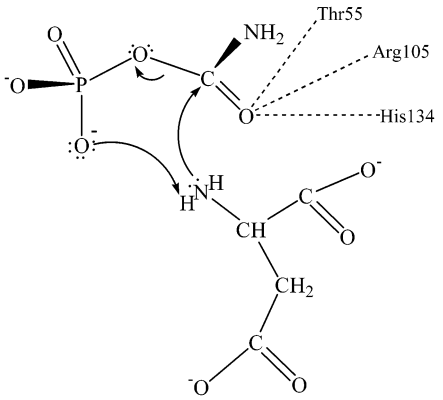

FIGURE 6: A Probable mechanism for catalysis by ATCase in which the critical removal of the proton from the NH_2 group of aspartate is accomplished by the leaving phosphate dianion. The carbonyl oxygen of the amide is bound to His134, Thr55, and Arg105.

tetrahedral, it has no amino group, and the P atom is joined by CH_2 instead of oxygen. Even so, a proposed tetrahedral intermediate can be built within 0.5 Å of the atoms of PALA at the proposed active site (*29*) and improved at 2.1 Å resolution (*10*). In this proposed mechanism, the leaving phosphate accepts a proton from the NH_2 of aspartate, as a lone pair of this NH_2 forms a bond to the carbon of the amide group (Figure 6). An alternative proton acceptor is possibly the NH_2 of Lys84*. The K84N (*30*) mutant shows more than a 1200-fold reduction in k_{cat}. Also, Lys84* with its NH_3^+ group may be involved in final removal of phosphate after carbamylaspartate leaves (*10*). At least, the tetrahedral intermediate mechanism is supported by isotope tracer plus NMR studies that eliminate the formation of cyanic acid or carbamic acid as intermediates (*31*). This mechanism could equally well be obtained from the binding of PALA, or from the carbamyl phosphate plus succinate (*27*), or from the phosphonoacetamide plus malonate structures (*28*). Comparison of these two dual substrate analogue atomic positions with those of PALA has been presented previously (*27*, *28*). These structures can be regarded as "reaction coordinate analogues" a term used for reactions of small molecules (*32*), and for enzyme reactions (*33*, *34*), and similar to the near-attack configuration (NAC) (*35*−*37*).

The ATCase−citrate−phosphate structure in a difference electron density at the 5σ level of the $F_o - F_c$ map at 2.9 Å resolution shows a gap between the citrate and phosphate. A difference $F_o - F_c$ electron density (5σ) of ATCase−PALA structure at 2.46 Å resolution shows continuous density between the phosphate group and the rest of the PALA molecule; moreover, the PALA density remained continuous when the highest resolution data were truncated at 2.9 Å (data not shown). Thus, the difference electron density maps are consistent with the displacement of PALA by citrate and phosphate during preparation of the crystal of ATCase−citrate−phosphate complex.

The OH of citrate, bound to Lys84* and to an oxygen of phosphate, is not present in PALA or in substrates or their analogues (Figure 4). Nevertheless, the binding of the remainder of citrate to the enzyme and to phosphate is consistent with earlier studies of inhibitors and substrate analogues. Yet, the binding of products can be sometimes more closely related to product leaving than to their structures immediately after the catalytic step. The larger gap, of 4 Å, between the carbon of the 5-carboxylate and the nearest phosphate oxygen may be an indication of slight movement toward product leaving. In a concurrent study of the T form of ATCase bound to products carbamylaspartate and phosphate, a very different mode of binding will be described in the following paper in this issue.

ACKNOWLEDGMENT

We thank Dr. E. R. Kantrowitz for his help and advice. This work is based upon research conducted at the Cornell High Energy Synchrotron Source (CHESS), which is supported by the National Science Foundation under award DMR 97-13424, using the Macromolecular Diffraction at CHESS (MacCHESS) facility, which is supported by award RR-01646 from the National Institutes of Health, through its National Center for Research Resources. This study of the citrate-phosphate complex with ATCase was inspired by a similar study in space group P321 to 2.8 Å resolution (Gouaux, J. E., Ph.D. Thesis, Harvard University, September 1989, Harvard University), pp V-1 to V-17.

REFERENCES

1. Gerhart, J. C., and Pardee, A. B. (1962) Enzymology of control by feedback inhibition, *J. Biol. Chem. 237*, 891−896.
2. Wild, J. R., Loughrey-Chen, S. J., and Corder, T. S. (1989) In the presence of CTP, UTP becomes an allosteric inhibitor of aspartate transcarbamylase, *Proc. Natl. Acad. Sci. U.S.A. 86*, 46−50.
3. Collins, K. D., and Stark, G. R. (1971) Aspartate transcarbamylase: interaction with the transition state analogue *N*-(phosphonacetyl)-L-aspartate, *J. Biol. Chem. 246*, 6599−6605.
4. Swyryd, E. A., Seaver, S. S., and Stark, G. R. (1974) *N*-(phosphonacetyl)-L-aspartate, a potent transition state analogue of aspartate transcarbamylase, blocks proliferation of mammalian cells in culture, *J. Biol. Chem. 249*, 6945−6950.
5. Weber, K. (1968) New structural model of *E. coli* aspartate transcarbamylase and the amino acid sequence of the regulatory polypeptide chain, *Nature 218*, 1116−1119.
6. Wiley, D. C., and Lipscomb, W. N. (1968) Crystallographic determination of symmetry of aspartate transcarbamylase: studies of trigonal and tetragonal crystalline forms of aspartate transcarbamylase show that the molecule has a three-fold and a two-fold symmetry axis, *Nature 218*, 1119−1121.
7. Honzatko, R. B., Crawford, J. L., Monaco, H. L., Ladner, J. E., Edwards, B. F. P., Evans, D. R., Warren, S. G., Wiley, D. C., and Ladner, R. C., Lipscomb, W. N. (1982) Crystal and molecular structures of native and CTP-liganded aspartate carbamoyltransferase from *Escherichia coli*, *J. Mol. Biol. 160*, 219−263.
8. Stevens, R. C., Gouaux, J. E., and Lipscomb, W. N. (1990) Structural consequences of effector binding to the T state of aspartate carbamoyltransferase: crystal structures of the unligated and ATP- and CTP-complexed enzymes at 2.6 Å resolution, *Biochemistry 29*, 7691−7701.
9. Ke, H. M., Lipscomb, W. N., Cho, Y., and Honzatko R. B. (1988) Complex of *N*-(phosphonacetyl)-L-aspartate with aspartate carbamoyltransferase: X-ray refinement, analysis of conformational changes and catalytic and allosteric mechanisms, *J. Mol. Biol. 204*, 725−747.
10. Jin, L., Stec, B., Lipscomb, W. N., and Kantrowitz, E. R. (1999) *Proteins: Struct., Funct. Genet. 37*, 727−742.
11. Svergun, D. I., Barberato, C., Koch, M. H. J., Fetler, L., and Vachette, P.(1997) Large differences are observed between the crystal and solution quaternary structures of allosteric aspartate transcarbamylase in the R-state, *Proteins 27*, 110−117.
12. Fetler, L., and Vachette, P. (2001) The allosteric activator Mg-ATP modifies the quaternary structure of the R-state of *Escherichia coli* aspartate transcarbamylase without altering the T↔R equilibrium, *J. Mol. Biol. 309*, 817−831.
13. Nowlan, S. F., and Kantrowitz, E. R.(1985) Superproduction and rapid purification of E. coli aspartate transcarbamoylase and its catalytic subunit under extreme derepression of the pyrimidine pathway, *J. Biol. Chem. 260*, 14712−14716.

14. Xu, W., Pitts, M. A., Middleton, S. A., Kelleher, K. S., and Kantrowitz, E. R. (1988) Propagation of allosteric changes through the catalytic-regulatory interface of *Escherichia coli* aspartate transcarbamylase, *Biochemistry 27*, 5507−5515.
15. Porter, R. W., Modebe, M. O., and Stark, G. R. (1969) Aspartate Transcarbamylase: kinetic studies of the catalytic subunit, *J. Biol. Chem. 244*, 1846−1850.
16. Masood, R., and Venkitasubramanian, T. A. (1987) Role of various carbon and nitrogen sources in the regulation of enzymes of pyrimidine biosynthesis in *Mycobacterium smegmatis* TMC 1546, *Ann. Inst. Pasteur/Microbiol. 138*, 501−507.
17. Navaza, J. (1994) *AMoRe*: an automated package for molecular replacement, *Acta Crystallogr., Sect. A: Found. Crystallogr. 50*, 157−163.
18. Kleywegt, G. J., and Jones, T. A.(1998) Databases in protein crystallography, *Acta Crystallogr., Sect. D: Biol. Crystallogr. 54*, 1119−1131.
19. Brunger, A. T., Adams, P. D., Clore, G. M., DeLano, W. L., Gros, P., Grosse-Kunstleve, R. W., Jiang, J.-S., Kuszewski, J., Nilges, N., Pannu, N. S., Read, R. J., Rice, L. M., Simonson, T., and Warren, G. L. (1998) Crystallography and NMR system (CNS): A new software system for macromolecular structure determination, *Acta Crystallogr., Sect. D: Biol. Crystallogr. 54*, 905−921.
20. Jones, T. A., Zou, J.-Y., Cowan, S. W., and Kjeldgaard, M. (1991) Improved Methods for Building Protein Models in Electron Density Maps and the Location of Errors in these Models, *Acta Crystallogr., Sect. A: Found. Crystallogr. 47*, 110−119.
21. Laskowski, R. A., MacArthur, M. W., Moss, D. S., and Thornton, J. M. (1993) PROCHECK: A program to check the stereochemical quality of protein structures, *J. App. Crystallogr. 26*, 283−291.
22. Jones, S., and Thornton, J. M. (1996) Principles of Protein−Protein Interactions Derived From Structural Studies, *Proc. Natl. Acad. U.S.A. 93*, 13−20.
23. Luzzati, V.(1952) Traitement statistique des erreurs dans la determination des structures cristallines, *Acta Crystallogr. 5*, 802−810.
24. Delano, W. L. (2002) The PyMOL molecular graphic system, San Carlos, CA, Delano Scientific.
25. Kraulis, P. J. (1991) MOLSCRIPT: a program to produce both detailed and schematic plots of protein structures, *J. Appl. Crystallogr. 24*, 946−950.
26. Esnouf, R. M. (1999) Further additions to *MolScript* version 1.4, including reading and contouring of electron-density maps, *Acta Crystallogr., Sect. D: Biol. Crystallogr. 55*, 938−940.
27. Gouaux, J. E., and Lipscomb, W. N.(1988) Three-dimensional structure of carbamoyl phosphate and succinate bound to aspartate carbamoyltransferase, *Proc. Natl. Acad. U.S.A. 85*, 4205−4208.
28. Gouaux, J. E., and Lipscomb, W. N. (1990) Crystal structure of phosphonoacetamide ligated T and phosphonoacetamide and malonate ligated R states of aspartate carbamoyltransferase at 2.8 Å resolution and neutral pH, *Biochemistry 29*, 389−402.
29. Gouaux, J. E., Krause, K. L., and Lipscomb, W. N. (1987) The catalytic mechanism of *Escherichia coli* aspartate carbamoyltransferase: a molecular modeling study, *Biochem. Biophys. Res. Commun. 142*, 893−897.
30. Robey, E. A., Wente, S. R., Markby, D. W., Flint, A., Yang, Y. R., and Schachman, H. K. (1986) Effect of amino acid substitutions on the catalytic and regulatory properties of aspartate transcarbamoylase, *Proc. Natl. Acad. Sci. U.S.A. 83*, 5934−5938.
31. Waldrop, G. L., Urbauer, J. L., and Cleland, W. W. (1992) Nitrogen-15 isotope effects on nonenzymic and aspartate transcarbamylase catalyzed reactions of carbamyl phosphate, *J. Am. Chem. Soc. 114*, 5941−5945.
32. Bürgi, H. B., and Dunitz, J. D. (1983) From crystal statics to chemical dynamics, *Acc. Chem. Res. 16*, 153−161.
33. Christianson, D. W., and Lipscomb, W. N. (1988) Comparison of carboxypeptidase A and thermolysin: inhibition by phosphonamidates, *J. Am. Chem. Soc. 110*, 5560−5565.
34. Christianson, D. W., and Lipscomb, W. N. (1989) Carboxypeptidase A, *Acc. Chem. Res. 22*, 62−69.
35. Hur, S., and Bruice, T. C. (2002) The mechanism of catalysis of the chorismate to prephenate reaction by the *Escherichia coli* mutase enzyme, *Proc. Natl. Acad. U.S.A. 99*, 1176−1181.
36. Lightstone, F. C., and Bruice, T. C. (1996) Ground State Conformations and Entropic and Enthalpic Factors in the Efficiency of Intramolecular and Enzymic Reactions. 1. Cyclic Anhydride Formation by Substituted Glutarates, Succinate, and 3,6-Endoxo-Δ4-tetrahydrophthalate Monophenyl Esters, *J. Am. Chem. Soc. 118*, 2595−2605.
37. Bruice, T. C., and Lightstone, F. C. (1999) Ground State and Transition State Contributions to the Rate of Intramolecular and Enzymic Reactions, *Acc. Chem. Res. 32*, 127−136.

BI030213B